Chemical Engineering Science 137 (2015) 964–976

Contents lists available at ScienceDirect

Chemical Engineering Science

journal homepage: www.elsevier.com/locate/ces

Optimal design of adsorbents for NORM removal from produced water in natural gas fracking. Part 1: Group contribution method for adsorption

Pahola T. Benavides, Urmila Diwekar *

Center for Uncertain Systems: Tools for Optimization & Management (CUSTOM), Vishwamitra Research Institute, Crystal Lake, IL 60012, USA

HIGHLIGHTS

- We applied group contribution methods (GCM) to predict specific properties of adsorbent required.
- We estimated the thermodynamic properties such as the activity coefficients of adsorbents based on the proposed GCM.
- We compare the experimental adsorption capacity and the estimated adsorption capacities from the GCM.

GRAPHICAL ABSTRACT

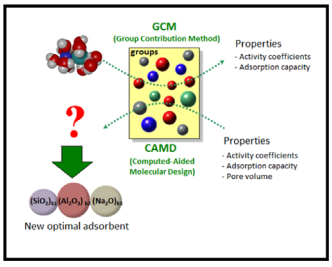

ARTICLE INFO

Article history:
Received 29 December 2014
Received in revised form
10 June 2015
Accepted 10 July 2015
Available online 26 July 2015

Keywords:
Natural gas
Hydraulic fracturing
Produced water
Natural occurring radioactive material (NORM)
Group contribution method (GCM)
Adsorbate solid solution theory (ASST)

ABSTRACT

Natural gas has become an essential energy resource in the U.S. due to the increasing demand of energy, the high oil prices, and the need of foreign oil independency. The improvement in the drilling technology has allowed the rapid expansion in gas production, especially for unconventional gas such as shale gas. Shale gas is natural gas trapped within fine-grained sedimentary rocks called shale formations. Hydraulic fracturing is used to extract natural gas from these formations. Although natural gas is cleaner-energy source than coal or oil, there is a lot of controversy due to the environmental impact related to the water consumption and treatment. Hydraulic fracturing generates significant volumes of wastewater that contain dissolved chemicals, high content of salts, and significant levels of natural occurring radioactive material (NORM). Hence, one of the biggest challenges of this industry is to develop techniques for the prevention, remediation, and appropriate disposal of NORM. The overall objective of this work is to develop and implement a novel computational tool for high-throughput screening and selection of new adsorbents for NORM removal. In the first part of this paper series, we study the adsorption theory for NORM removal and applied group contribution methods (GCMs) to predict specific properties of adsorbents based on their thermodynamics. Then, in the second part of this paper we develop a computer-aided molecular design (CAMD) framework that generates potential adsorbent candidates according to the properties developed by the GCMs.

© 2015 Elsevier Ltd. All rights reserved.

1. Introduction

The increase of the world's energy demand and the high oil prices has led to the exploration of new resources such as the extraction of natural gas from unconventional shale plays like

* Corresponding author.
E-mail address: urmila@vri-custom.org (U. Diwekar).

http://dx.doi.org/10.1016/j.ces.2015.07.012
0009-2509/© 2015 Elsevier Ltd. All rights reserved.

shale gas. Natural gas production from shale gas formation is one of the fastest-growing divisions in the U.S. oil and gas industry, and it is a promising resource to achieve the foreign oil independency. The U.S. Energy Information Administration estimates U.S natural gas reserves at 2203 trillion cubic feet (tcf), enough to last about 92 years (U.S. Department of Energy Website, 2014a, 2014b). Advances in drilling technology have rapidly expanded natural gas production. According to a reference case reported on the Annual Energy Outlook of 2014 (U.S. Department of Energy Website, 2014a, 2014b), the production of natural gas will grow steadily, with a 56% increase between 2012 and 2040, when production will reach 37.6 tcf. This substantial growth in shale gas production comes with new environmental concerns.

Shale gas is a natural gas trapped within fine-grained sedimentary rocks called shale formations. Two important shale plays are the Barnett Shale in Texas and the Marcellus Shale in the eastern of the U.S which is shown in Fig. 1 (Replica Engineering INC, 2014). It was deposited around 390 million years ago in the shallow sea that once covered the region. Shale is composed of tiny mud particles and organic matter, which, because of the properties of radioactive elements present in the sea water, often contains concentrations of naturally occurring radioactive material (NORM). Black shale, such as that contained in the Marcellus, often contains trace levels of uranium (U), thorium (Th), and potassium (K), and in higher concentrations than found in less organic-rich gray shale. Natural gas fracking in the Marcellus shale brings out NORM to the surface in a concentrated form, which could pose a radiation safety hazard and it is the focus of these series of papers.

The first stage of shale gas production requires large volumes of fresh water (e.g. 4–5 million of gallons according to Smith (2012)) that may affect the availability of water for other uses as well as aquatic habitats. About 15–25% of the water injected during hydraulic fracturing returns to surface as "flowback water" within the first 30 days while produced water, which is the water produced at the end of the flowback, continues to flow for the life of the well at a reduced rate (Silva et al., 2012). Moreover, hydraulic fracturing generates significant volumes of contaminated wastewater which may contain dissolved chemicals and other contaminants that require a special treatment before final disposal or reuse. In Marcellus gas shale, the overall estimated volume of wastewater (3.1×10^6–3.8×10^6 cubic meter per year) has increased during the last years and there is an average of 0.15–0.3 MM gallons per day of produced water that must be properly disposed (Silva et al., 2012). It has been found that the salinity of shale gas wastewater varies from 5000 mg/L to $>$200,000 mg/L (Warner et al., 2013). Much of the flowback and produced waters such as those generated in the Marcellus contain

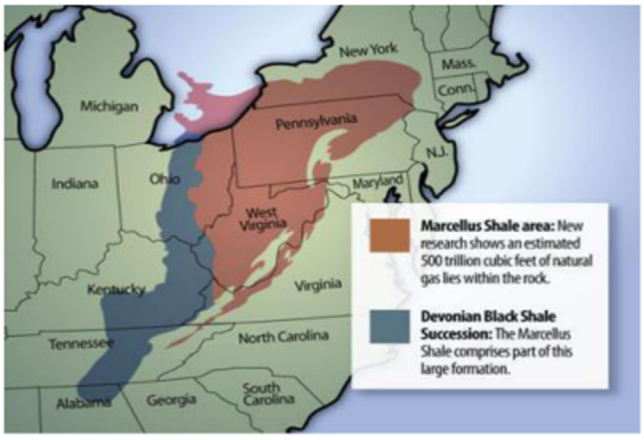

Fig. 1. Marcellus shale the Marcellus is a gas-bearing shale formation that ranges geographically from Ohio and West Virginia into Pennsylvania and southern New York.

concentrated amount of hardness species (e.g. Ca^{++}, Mg^{++}, Mn^{++}, Br^{++}, and Cl^{-}) and metals such as barium and strontium. As stated earlier, added to this high salinity, many flowback and produced waters contain significant levels of NORM in the form of radium isotopes with activities of 185–592Bq/L (Warner et al., 2013). Although 95% of the flowback water is reused, the supply of flowback and produced water is expected to exceed the reuse capacity due to the rapid increase in shale gas extraction. This situation has become a big issue in the safe disposal of liquid waste in the U.S. given their large volume and typically high levels of contaminants. Most oil–gas field NORM waste is stored at production sites awaiting for disposal in specially designated and permitted landfills, disposal wells, injections wells, or treat it in a publicly owned treatment plant or wastewater treatment plants. If the production site cannot handle the final disposal of these waters, then these waters must be sent to other water treatment facilities which increase the costs of operation. However, as the natural gas production increases, these alternatives will not be enough to support its final –safe-disposal. In some states, these alternatives are not available or allowed due to the lack of regulations or appropriate geology for deep-well injection sites. Moreover, there is still potential for drinking water contamination due to spill in the surface and leaks from improperly cemented well casting. Even though multiple layers of steel casting are inserted into the wellbore to avoid contamination, there has been found some documented cases of localized releases of fluids at the surface causes by spill and casting ruptures (Lustgarten, 2009). Therefore, one of the biggest challenges of this industry is to develop techniques for the prediction, prevention, remediation, and appropriate disposal of oil-field NORM. Currently, it is not possible to selectively remove NORM from produced water so that brines could be reduced in volume to concentrated salt solutions or dry salts producing a waste material that does not have radionuclide safety issues.

In this work, we concentrate on the adsorption process for NORM removal specifically the radium and barium isotopes. Computer-aided molecular design (CAMD) is used to develop new adsorbents with desired properties that can remove these materials. CAMD is generally the reverse use of the group contribution method (GCM) that is used to generate molecules having desirable properties. A GCM is a technique to estimate and predict thermodynamic and other properties from molecular structures of compounds. In the first part of this paper, we focus on developing group GCMs to predict the desired properties based on their thermodynamics. We use experimental data of known adsorbents and their adsorption equilibrium to predict the properties such as activity coefficient. A modified UNIFAC method is used for calculation of activity coefficient. In the second part of this paper (Benavides et al., 2015), we use CAMD framework to generate new adsorbent having the desirable properties. As a result, the GCM along with CAMD based optimization methods identify existing and new potential groups of adsorbents for the NORM removal.

2. Background

2.1. Natural occurring radioactive material (NORM)

The natural environment contains many naturally radioactive substances also known as NORM that emit low levels of radiation. Among some radioactive material are: uranium (U), radium (Ra), thorium (Th) and radon (Rn). These elements are found dissolved in very low concentration during normal reactions between water and rock or soil that also contain oil and gas (Zielinski and Otton, 1999). As stated earlier, the black shale found at Marcellus shale often contains trace levels of radioactive material (^{238}U, ^{235}U, and ^{232}Th) which are brought out to the surface in a concentrated form. ^{238}U and ^{232}Th are both potentially hazardous radioactive products since they decay to more soluble ^{226}Ra and soluble ^{228}Ra,

respectively (Marcellus Shale, 2011). On the other hand, it has been found that mixtures of carbonate and sulfate minerals are present in the coating and sediments in the production equipment. One of these sulfate minerals is Barite (i.e. Barium Sulfate), which is known as the primary host NORM (Zielinski and Otton, 1999). Therefore, the focus of this work is on the adsorption of NORM specifically radium and barium isotopes.

Radium (Ra) is a radioactive element that may represent a potential health hazard (i.e. as carcinogen and other disorders) if it is released into the environment because radium and its decays product radon emit alpha particles that can kill and mutate cells. In produced water, NORM species typically comprise two forms: ^{226}Ra and ^{228}Ra (Zielinski and Otton, 1999). Due to the long half-life of 1600 years, ^{226}Ra is of principal interest compared to ^{228}Ra which has a half-life of 5.8 years. Although it is expected that both forms will behave similarly in the removal process, we focus on the adsorption of ^{228}Ra. Radioactive isotopes are commonly quantified in terms of activity concentration or simply "activity". These concentrations are generally reported as picocuries/gram (pCi/g) of solid material or picocuries/liter (pCi/L) of water or air. A picocurie equals 0.037 Bq which is another form to express the activity. Marcellus shale produced water samples contain more radium than non-Marcellus samples. For instance, the range of radium activities for samples from Marcellus shale (median value is 2460 pCi/L) overlaps the range for non-Marcellus reservoirs (median value 734 pCi/L) (Rowan et al., 2011).

Barium is a major fission product resulting from the fission of plutonium and uranium. High concentration of barium has been associated with multiple sclerosis and neurodegenerative diseases (Purdey, 2004). The toxicity of barium is related to its solubility and for insoluble salts the solubility increases with decreasing pH. The EPA allows a maximum of 0.002 mg/g of barium in drinking water (U.S.EPA, 2014).

2.2. Adsorption process

Adsorption is a separation process consists adhesion of molecules of liquids, gases and dissolved substances (i.e. adsorbate) into the surface of solid (i.e. adsorbent) because of physical and chemical processes (Yang, 2003). The most fundamental property in adsorption is the adsorption equilibrium which can be describe by adsorption isotherms (Suzuki, 1990). The isotherms are illustrated in many mathematical forms such as the Langmuir shown in Eq. (1):

$$\frac{1}{q}=\frac{1}{b}+\frac{1}{(bK)C} \tag{1}$$

where q the amount adsorbate adsorbed in a unit mass of adsorbent and C is the equilibrium concentration of adsorbate in the solution. b and K are constant values. Another typical equation used to describe the isotherm is the Freundlich equation as shown in Eq. (2). In this case, k_f and n_f are the Freundlich parameters determined from correlation of adsorption data.

$$q = k_f C^{n_f} \tag{2}$$

Adsorption can perform many separations that are impossible or impractical by conventional techniques such as distillation, absorption, and even membrane-based systems. However, adsorption is rarely employed as a separation process due to the lack of both experimental data and suitable models used to predict the equilibrium behavior of multicomponent mixtures (Berti et al., 2000). In addition, the calculation of the measurements involved in the equilibrium is very time-consuming and cost-intensive. Therefore, distillation processes have assumed a dominant role in separation technology. GCM method has shown a great success for the design of the most common separation processes and similar approaches are suggested for the calculation of adsorption processes.

2.3. Adsorbate solid solution theory (ASST)

In contrast to the classical formulation of adsorption equilibrium, the adsorbate solid solution theory (ASST) describes the adsorption behavior of liquid mixtures on solid surfaces using G^E-models (i.e. Gibbs excess free energy models). The approach, discussed by Berti et al. (1999, 2000) considers the adsorbed phase to be a mixture containing the adsorbed species and the adsorbent as additional component (see Fig. 2a). The relation of the phase equilibrium for component i is shown in Eq. (3):

$$x_i^b \gamma_i^b = x_i^s \gamma_i^s \exp\left(\frac{g^{ad}-g_{oi}^{ad}}{RT\Gamma_{mi}^s}\right) \tag{3}$$

Here, x_i^b and x_i^s are the fractions of component i in the bulk phase and surface phase, respectively. γ_i^b and γ_i^s are the activity coefficients in each phase, g^{ad} is the free energy of immersion of the adsorbed solution and g_{oi}^{ad} is the free energy of immersion of the pure adsorbed species i. T, R and Γ_{mi}^s are temperature, the ideal gas constant, and surface phase capacity of component i,

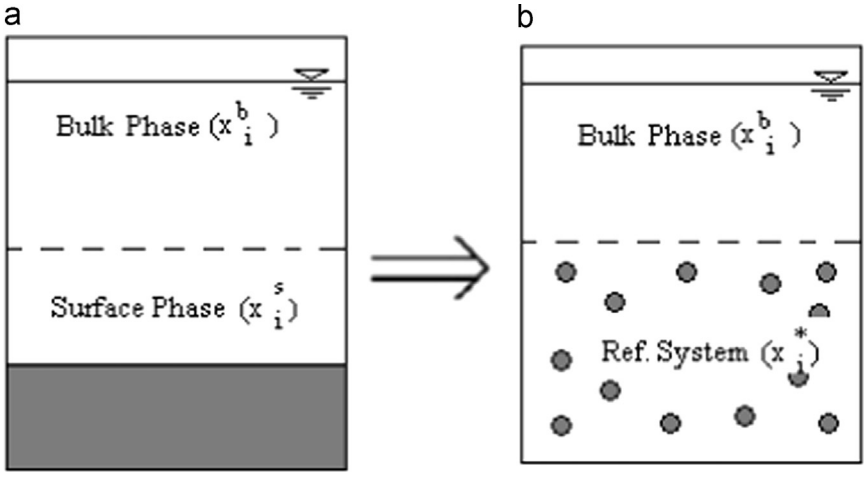

Fig. 2. Classical description of the adsorption systems (a) the total amount of fluid molecules is divided in two independent phases that are assumed to be homogeneous: the adsorbed or surface phase and the bulk phase. The adsorbate solid solution (b) is defined as the reference system and the bulk phase is considered to be uninfluenced by the solid

respectively (Berti et al., 1999, 2000). The surface phase capacity Γ^{s}_{mi} is given by Eq. (4), when assuming pore-filling model of adsorption, vp is the pore volume of the adsorbent and v_{oi} is the molar volume of the respective fluid:

$$\Gamma^{s}_{mi} = \frac{vp}{v_{oi}} \tag{4}$$

Berti et al. (1999, 2000) argued that for the pure component adsorption, the respective activity coefficient equals to 1, however, the measurable enthalpy of immersion proves the existence of interactions between adsorbent and the liquid. Therefore, they formulated a new thermodynamic framework that incorporates the adsorbent's properties by conceiving adsorption systems as a solution of the solid and the liquid adsorbates. In that sense, the influence of different structural groups of the adsorbent on the adsorption behavior is taken into account. This framework is described in Fig. 2b (Berti et al., 2000). Then, the relation of the phase of equilibrium for this new framework is presented by Eq. (5) based on the chemical potential in both phases.

$$x^{b}_{i}\gamma^{b}_{i} = x^{*}_{i}\gamma^{*}_{i}\exp\left(\frac{(\varphi^{*}-\varphi^{*}_{oi})}{RT\Gamma^{s}_{mi}}\right) \tag{5}$$

where x^{*}_{i} is the fraction of component i in the adsorbate solid solution, γ^{*}_{i} is the activity coefficient of the same component, and the expression $(\varphi^{*}-\varphi^{*}_{oi})$ is the difference between the chemical potential of the wetted solid and the chemical potential of the wetted solid at adsorption of the pure component i (Berti et al., 1999, 2000). This last term can be computed by Eq. (6)

$$\phi^{*}-\phi^{*}_{oi} = \frac{1}{m_0}\left(G^{E*}-G^{Es}-G^{E*}_{0i}\right) \tag{6}$$

Here, m_0 is the mass of adsorbent, and $G^{E*}, G^{Es}, G^{E*}_{0i}$, are the Gibbs excess free energy of the ASS, Gibbs excess free energy of the surface phase and the Gibbs excess free energy of the pure component adsorption all in Joules, respectively. Usually, it is more convenient to express the Gibbs excess free energy in terms of activity coefficients, therefore, for the adsorbate solid solution:

$$\frac{G^{E*}}{RT} = \sum_{i=0}^{k} n^{*}_{i}\ln\gamma^{*}_{i} \tag{7}$$

where the index 0 refers to the adsorbent and the activity coefficient is computed using the UNIFAC model (Berti et al., 1999).

Similarly, the definition of the activity coefficients for the surface phase yields their connection with the Gibbs excess free energy as shown below:

$$\frac{G^{Es}}{RT} = \sum_{i=1}^{k} n^{s}_{i}\ln\gamma_{i}(x^{s}_{i}) \tag{8}$$

where n^{s}_{i} is the molar quantity in the surface phase for component i and it is computed using the following equation:

$$n^{s}_{i} = x^{s}_{i}n^{*}_{T}(1-x^{*}_{0}) \tag{9}$$

and x^{s}_{i} (fraction of component i in the surface phase) can be calculated by:

$$x^{s}_{i} = \frac{x^{*}_{i}}{(1-x^{*}_{0})} \tag{10}$$

Finally, for the pure component adsorption, the respective activity coefficient γ^{*}_{oi} is given by Eq. 11:

$$\gamma^{*}_{oi} = 1+\frac{1}{\Gamma^{s}_{mi}M_o} \tag{11}$$

2.4. Group contribution method (GCM) and the modified UNIFAC model

GCM is used to estimate properties of compounds based on known experimental data of well-defined pure components and mixtures. Many examples can be found in the literature (Lydersen, 1955; Joback and Reid, 1987; Marrero and Gani, 2001). The objective of GCMs is formulating a property of a given compound as a statistical correlation like multi-linear regression. The parameters involved in this regression are determined by summing the frequency of each group occurring in the molecule times its contribution. The ASST offers an excellent basis to incorporate group contribution methodology that takes into account the influence of different structural groups of the adsorbent with respect to adsorption. This theory uses the UNIFAC method which is also used to predict information for the vapor–liquid equilibrium (Fredenslund et al., 1977). UNIFAC stands for functional-groups activity coefficients and this method is resulted from the model called UNIQUAC (Universal Quasi-Chemical). Thus, for the first evaluation of a group contribution method, a modified UNIFAC model presented by Berti et al. (2000) is used to compute the activity coefficient in the adsorbent solid solution. In the modified model, the pure component adsorption (γ^{*}_{oi}) has to be incorporated as shown in Eq. (12):

$$\ln\gamma^{*}_{i} = \ln\gamma^{*}_{oi} + \ln\gamma^{*}_{GE,i} \tag{12}$$

where $\gamma^{*}_{GE,i}$ is the concentration dependant part of the activity coefficient and it is divided into a combinatorial part (γ^{C*}_{i}) and residual part (γ^{R*}_{i}):

$$\ln\gamma^{*}_{GE,i} = \ln\gamma^{C*}_{i} + \ln\gamma^{R*}_{i} \tag{13}$$

For the combinatorial and residual part Eqs. (14) and (15) can be used:

$$\ln\gamma^{C*}_{i} \equiv \ln\gamma^{C*}_{GE,i}(x^{*}_{i}) - \ln\gamma^{C*}_{GE,i}(x^{*}_{0i}) \tag{14}$$

$$\ln\gamma^{R*}_{i} \equiv \ln\gamma^{R*}_{GE,i}(x^{*}_{i}) - \ln\gamma^{R*}_{GE,j}(x^{*}_{0i}) \tag{15}$$

For the adsorbent each of the second terms is dropped. The combinatorial and the residual part is given as it is presented by Fredenslund et al. (1977). $\gamma^{*}_{GE,i}(x^{*}_{0i})$ represents the activity coefficient of a binary ASS, that is, the pure adsorbed liquid and the adsorbent.

3. Adsorption of radium and barium

In this section, we study the adsorption equilibrium of radium and barium on different adsorbents. Based on experimental data reported in the literature, we predict the interaction parameters of the functional groups that are commonly contained in adsorbents of radium and barium.

3.1. Problem description of radium removal

The first problem considers the adsorption of radium from aqueous solutions on different minerals. The experimental data was reported by Ames et al. (1983a, 1983b). In the paper, the authors presented radium adsorption efficiencies as a function of temperature determined in a 0.01 M NaCl solution. In the initial solution, when no adsorbent is added, the components involved are: radium (1), sodium chloride (2), and water (3). The equilibrium is reached after 30 days of mineral solution continuous contact. At this point, two new phases are presented: bulk phase and the adsorbate solid solution (see Fig. 2b). The bulk phase contains part of the radium that was not adsorbed, sodium

chloride, and water while in the ASS phase contains the adsorbed radium and the adsorbent as shown in Fig. 3.

Table A3 of Appendix 3 presents the minerals used by Ames et al. (1983a, 1983b) with their properties which used the Freundlich equation (Eq. 2) to describe the adsorption equilibrium. The values of k and n are given by Ames et al. (1983a, 1983b). These values depend on the temperature and type of adsorbent. Therefore, for the purpose of this paper we use the information reported at 25 °C of adsorption temperature for experimental results.

3.2. Mass balance of the adsorption process

The first two quantities that can be compute with the given information are the moles of adsorbent n_0^* and radium n_1^* in the ASS, as it is presented in Eqs. (16) and (17), respectively:

$$n_0^* = \frac{m_0}{M_0} \tag{16}$$

$$n_1^* = q{*}m_0 \tag{17}$$

Then, the amount of radium in the bulk phase (n_1^b) is determined by subtracting the moles of radium contained in the solid (n_1^*) from the initial feed of moles contained in the solution (n_1^1):

$$n_1^b = n_1^1 - n_1^* \tag{18}$$

where n_1^1 is calculated with Eq. 19. C_I(mol/L) is the initial concentration of radium and V_{sln} as the volume of solution (1 L from which 0.88 L were water):

$$n_1^1 = C_I V_{sln} \tag{19}$$

Finally, the molar fractions of radium, NaCl, and H_2O in the bulk phase (x_i^b) can be computed as presented in Eq. (20):

$$x_i^b = \frac{n_i^b}{n_T^b} \quad \forall\ i \in [1\ldots3] \tag{20}$$

The molar fraction of radium and adsorbent in the ASS phase (x_i^*) can be calculated as presented in Eq. (21):

$$x_i^* = \frac{n_i^*}{n_T^*} \quad \forall\ i \in [0 \text{ and } 1] \tag{21}$$

where n_T^b and n_T^* are the total moles in the bulk phase and in the ASS, respectively.

3.3. Activity coefficient for bulk phase and adsorbate solid solution

As mentioned before, the UNIFAC model is divided in two parts: combinatorial and residual. In the case of bulk phase, Eq. (22) can be written as:

$$\ln \gamma_i^b = \ln \gamma_i^{Cb} + \ln \gamma_i^{Rb} \tag{22}$$

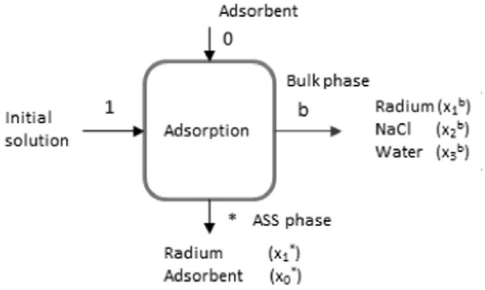

Fig. 3. Flowchart of adsorption of radium. In this figure "1" represents the initial solutions, "0" represents the adsorbent added, "b" is the bulk phase and "*" is the adsorbate solid solution (ASS) phase.

For combinatorial part of component i:

$$\ln(\gamma_i^{Cb}) = \ln\left(\frac{\varphi_i}{x_i^b}\right) + 5q_i \ln\left(\frac{\theta_i}{\varphi_i}\right) + l_i - \frac{\varphi_i}{x_i^b}\sum_1^j x_j^b l_j \tag{23}$$

where

$$l_i = 5(r_i - q_i) - (r_i - 1) \tag{24}$$

$$\theta_i = \frac{q_i x_i^b}{\sum_j^M q_j x_j^b} \tag{25}$$

$$\varphi_i = \frac{r_i x_i^b}{\sum_j^M r_j x_j^b} \tag{26}$$

$\overline{\theta}_i$ and φ_i represent the molecular surface area and volume fraction of species i, respectively, and $j: 1,2\ldots M$ represent the number of components. The van der Waals volume species/functional group/component is computed by Eq. (27) while the van der Waals surface area using Eq. (28), respectively:

$$r_i = \sum_g^{N_{gt}} \vartheta_g^{(i)} R_g \tag{27}$$

$$q_i = \sum_g^{N_{gt}} \vartheta_g^{(i)} Q_g \tag{28}$$

In this case, $g = 1,2\ldots N_{gt}$, g is the groups index and N_{gt} total functional group in the molecule. R_g and Q_g are the constants of group sizes and surface areas that are obtained from atomic and molecular structure data. The R_g and Q_g can be viewed in Table A1 of Appendix 1.

For residual part for group k:

$$\ln \Gamma_g = Q_g\left[1 - \ln\left(\sum_1^m \theta_m \psi_{mg}\right) - \sum_1^m \left(\frac{\theta_m \psi_{gm}}{\sum_1^n \theta_n \psi_{nm}}\right)\right] \tag{29}$$

where m and n represent all groups. Eq. (29) also holds to $\Gamma_g^{(i)}$

The group fraction and group surface area fraction is calculated by Eqs. (30) and (31), respectively:

$$X_m = \frac{\sum_1^j \vartheta_m^{(i)} x_j^b}{\sum_1^j \sum_1^n \vartheta_m^{(i)} x_j^b} \tag{30}$$

$$\theta_m = \frac{Q_m X_m}{\sum_1^n Q_n X_m} \tag{31}$$

Finally, in Eq. 29 the parameter ψ_{nm} is given by:

$$\psi_{nm} = \exp(-a_{nm}/T) \tag{32}$$

a_{nm} contains the group interaction parameters for the UNIFAC model and T is the temperature. The group interaction parameter is the measure of the difference in the energy of interaction between a group n and a group m and between two same groups m (Fredenslund et al., 1977). Table 1 presents the known and unknowns values of a_{nm} for the groups used. As it can be seen, there are 6 unknown interaction parameters in which all of them are related to radium group.

To compute the activity coefficient for the adsorbate solid solution (γ_i^*), the UNIFAC model presented in Section 2.3 is used. Table A2 of Appendix 2 presents the van der Waals volume and surface values for each functional group of the different adsorbents used. On the other hand, Table 2 shows the interaction parameters involved in the ASS where there are 14 unknown interaction parameters in which all of them are related to radium group. According to Berti et al. (1999) the interaction parameters between the groups on the solid are zero.

3.4. Problem description for barium removal

Produced water can also contain barium at high concentration. Therefore, in order to reach high efficiency of the recovery of water, the barium must be removed. The experimental data was obtained from two papers: Chavez et al. (2010) and Arafa et al. (1974). In the first paper, the adsorption isotherms were determined by contacting 0.2 g of two adsorbents: clinoptilolite tuff and montmorillonite clay with 10 ml of a solution that contained barium chloride ($BaCl_2$) and calcium chloride ($CaCl_2$). Similarly to radium adsorption, two phases are presented after reaching equilibrium (See Fig. 4). The second paper by Arafa et al. (1974) – 5 g of adsorbent were mechanically shaken with 100 cm^3 of a solution of barium chloride and sodium chloride (0.01 M) for three hours. Fig. 4 can also be used to represent the adsorption scheme process presented by Arafa et al. (1974). However, in the latter case, the adsorbent used was the β-Mn_2O and the bulk phase composition contained barium chloride that did not react, sodium chloride and water. Table A4 in Appendix 3 presents the chemical structure of the adsorbents used for adsorption of radium and their molecular weight.

The adsorption equilibrium of Ba^{+2} by Ca-Cln and by Ca-Mnt are described by the Langmuir equation shown in Eq. 1. The constant values of *b* and *K* can be found in Chavez et al. (2010). On the other hand, the adsorption equilibrium of barium by β-Mn_2O is taken from the adsorption isotherm presented in the paper by Arafa et al. (1974). Its isotherm was of the Langmuir type and it was reported at pH 7.5 and 35 °C of temperature. We use the same procedure presented for radium adsorption to estimate the moles and mole fractions in the bulk and ASS phase. Table 3 presents the known and unknown values of interaction parameters based on the groups used in each problem in the bulk phase (ab_{nm}). The van der Waals volume and surface parameters for each functional group can be found in Table A1 of Appendix 1. As it can be seen in these tables, there are four unknown interaction parameters in each problem, in which all of them are related to barium group.

Finally, Table 4 shows the interaction parameters involved in the ASS phase (aa_{nm}) for the two adsorption problems, respectively. For problem one (i.e. barium adsorption onto Ca-Cnt and Ca-Mnt) there are 20 unknowns while for problem two (i.e. barium adsorption onto β-Mn_2O) there are only two unknowns (i.e. aa_{112} and aa_{121}). The optimization problem presented in the main paper was used to find these interaction parameters.

Table 1
UNIFAC interaction parameters (ab_{nm}) for bulk phase.

Groups (g)	Ra	Na^+	Cl^-	H_2O
Ra	0	ab_{12}	ab_{13}	ab_{14}
Na^+	ab_{21}	0	6342.2[a]	−165.0[a]
Cl^-	ab_{31}	14548[a]	0	−230.2[a]
H_2O	ab_{41}	22.38[a]	−982.5[a]	0

[a] The known values of a_{nm} can be found in Kikic and Fermeglia (1991).

Table 2
UNIFAC interaction parameters (aa_{nm}) for ASS.

Groups (g)	Ra	SiO_2	Al_2O_3	Na_2O	MgO	Fe_2O_3	K_2O	CaO
Ra	0	aa_{12}	aa_{13}	aa_{14}	aa_{15}	aa_{16}	aa_{17}	aa_{18}
SiO_2	aa_{21}	0	0	0	0	0	0	0
Al_2O_3	aa_{31}	0	0	0	0	0	0	0
Na_2O	aa_{41}	0	0	0	0	0	0	0
MgO	aa_{51}	0	0	0	0	0	0	0
Fe_2O_3	aa_{61}	0	0	0	0	0	0	0
K_2O	aa_{71}	0	0	0	0	0	0	0
CaO	aa_{81}	0	0	0	0	0	0	0

4. Estimation of the interaction parameters: an optimization problem

As mentioned before, our objective is to find the unknown values of the UNIFAC interaction parameters (i.e. ab_{nm} and aa_{nm}) by fitting different adsorption systems and compared them with the information found in the literature. Therefore, we use optimization techniques to solve the two parameter estimation problems presented in the previous section (i.e. radium and barium adsorption). The parameter estimation problem deals with solving a system of equations based on measured or empirical data so that the values of the parameters can be estimated by optimizing an objective function. We use an error function (Err) (mean square error) as an objective function for this problem. This function represents the square root of the difference between the adsorption capacity from the experimental values (q^{exp}) given by the adsorption equilibrium and a new calculated q^{cal}. This adsorption capacity difference is applied for each adsorbent used. For the radium adsorption problem, we considered 4 adsorbents (Kaolinite, montmorillinite, glauconite, and clinoptinolite) since they contain all the functions group needed for the prediction of the interaction parameters. For the barium adsorption problem, we solved two problems: adsorption of barium onto Ca-Cln and Ca-Mnt and adsorption of barium onto β-MnO_2. Then, using the interaction parameters as the decision variables, the objective function whose goal is to minimize the sum of this square of errors is expressed as:

$$\text{minErr} = \min \sum_{1}^{AD} \sum_{1}^{Eq} \left[q^{cal}_{Eq,AD} - q^{exp}_{Eq,AD} \right]^2 \tag{33}$$

where AD is the adsorbent used, and Eq is the total number of equation used to solve the problem, we used around 20–40 experimental data points (i.e. 20–40 equations) depending on

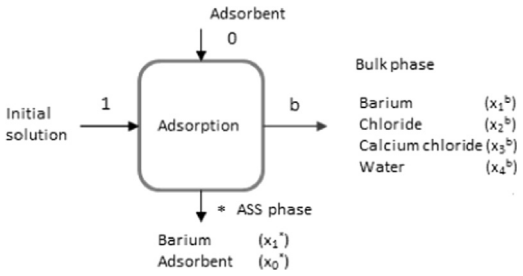

Fig. 4. Flowchart of adsorption of barium. In this case, the bulk phase contains part of the barium (1) that was not adsorbed, chloride ion (2), calcium chloride (3), and water (4) while in the ASS phase the adsorbed barium and the adsorbent (0) are the two components taken into account.

Table 3
UNIFAC interaction parameters (ab_{nm}) for bulk phase for adsorption of barium onto Ca-Cnt and Ca-Mnt and adsorption onto β-Mn_2O.

Groups (g)	Ba^{2+}	Ca^{2+}	Cl^-	H_2O	Na^+
Ba^{2+}	0	ab_{12}	ab_{13}	−558.57[a]	ab_{15}
Ca^{2+}	ab_{21}	0	4166.3[a]	−838.2[a]	NA[b]
Cl^-	ab_{31}	21983[a]	0	−230.2[a]	14548[a]
H_2O	−374.92[a]	−897.2[a]	−982.5[a]	0	22.38[a]
Na^+	ab_{51}	NA[b]	6342.2[a]	−165.0[a]	0

[a] The known values of ab_{nm} for can be found in Kikic and Fermeglia (1991).
[b] There is not interaction parameter between Na and Ca since each of them belongs to different adsorption problem.

Table 4
UNIFAC interaction parameters (ab_{nm}) for ASS phase onto Ca-Cln and onto Ca-Mnt and onto β-Mn_2O.

Groups (g)	Ba^{2+}	SiO_2	Al_2O_3	$(AlO_2)^-$	FeO	MgO	CaO	Na_2O	K_2O	Ca^{2+}	K^+	β-MnO_2
Ba^{2+}	0	aa_{12}	aa_{13}	aa_{14}	aa_{15}	aa_{16}	aa_{17}	aa_{18}	aa_{19}	aa_{110}	aa_{111}	aa_{112}
SiO_2	aa_{21}	0	0	0	0	0	0	0	0	0	0	NA[a]
Al_2O_3	aa_{31}	0	0	0	0	0	0	0	0	0	0	NA[a]
$(AlO_2)^-$	aa_{41}	0	0	0	0	0	0	0	0	0	0	NA[a]
FeO	aa_{51}	0	0	0	0	0	0	0	0	0	0	NA[a]
MgO	aa_{61}	0	0	0	0	0	0	0	0	0	0	NA[a]
CaO	aa_{71}	0	0	0	0	0	0	0	0	0	0	NA[a]
Na_2O	aa_{81}	0	0	0	0	0	0	0	0	0	0	NA[a]
K_2O	aa_{91}	0	0	0	0	0	0	0	0	0	0	NA[a]
Ca^{2+}	aa_{101}	0	0	0	0	0	0	0	0	0	0	NA[a]
K^+	aa_{111b}	0	0	0	0	0	0	0	0	0	0	NA[a]
β-MnO_2	aa_{121}	NA[a]	NA[a]	NA[a]	NA[a]	NA[a]	NA[a]	NA[a]	NA[a]	NA[a]	NA[a]	0

[a] There is not interaction parameter between β-MnO_2 and the other groups since β-MnO_2 belongs to the second problem by Arafa et al. (1974).

the problem. To calculate q^{cal}, we use Eq. (34):

$$q^{cal} = \frac{x_1^* \; n_T^*}{m_0} \tag{34}$$

To find n_T^*, we use the equations of the adsorption equilibrium formulation presented in the previous sections which include the equilibrium equation (Eq. (5)) and the difference of the chemical potential of the adsorbent (Eq. (6)). This last equation involves the calculation of the Gibbs excess free energy in three parts: adsorbate solid solution (Eq. (35)), surface phase (Eq. (36)), and for the pure component (Eq. (37))

$$G^{E*} = RT\left(n_0^* \ln \gamma_0^* + n_1^* \ln \gamma_1^*\right) = RT\left(x_0^* \, n^* \ln \gamma_0^* + x_1^* n^* \ln \gamma_1^*\right) \tag{35}$$

$$G^{Es} = RT\left(n_1^s \ln \gamma_1(x_1^s)\right) = RT\left(n^s x_1^s \ln \gamma_1(x_1^s)\right) \tag{36}$$

$$G_{0i}^{E*} = RT n_{0i}^* \ln \gamma_{0i}^* = RT x_{0i}^* n^* \ln\left(1 + \frac{1}{\Gamma_{mi}^s M_0}\right) \tag{37}$$

where $x_{0i}^* = x_1^*$ since there only one adsorbate (either radium or barium) in the ASS phase. G^{Es} is the Gibbs excess free energy of the surface phase and in this case is equal to zero since only involves the activity coefficient for pure component ($x_1^s = 1$), therefore, replacing Eqs. 34, 35 and 36 into Eq. (6), we obtain an expression to calculate n_T^*:

$$n_T^* = \frac{\left(\phi^* - \phi_{oi}^*\right) m_0}{RT\left(\left(x_0^* \ln \gamma_0^* + x_1^* \ln \gamma_1^*\right) - x_{01}^* \ln\left(1 + \frac{1}{\Gamma_{m1}^s M_o}\right)\right)} \tag{38}$$

The surface phase capacity Γ_{mi}^s is given by Eq. (4). The pore volume values of the adsorbents used are listed in Table A2 of Appendix 2. Finally, to compute $(\phi^* - \phi_{oi}^*)$, if Eq. (5) is used, then:

$$\varphi^* - \varphi_{oi}^* = -R\,T\,\Gamma_{mi}^s \ln\left(\frac{x_i^b \gamma_i^b}{x_i^* \gamma_i^*}\right) \tag{39}$$

The nonlinear programming (NLP) optimization solution methods are used to determine the UNIFAC interaction parameters using Matlab software. As an example, we present the calculation steps to compute the adsorption capacity for Kaolinite in Appendix 4 (Tables A5 and A6).

We used the nonlinear least square fit for this purpose. We took 41 experimental points and converted it into a single objective function of sum error square between these experimental values and calculated values. We applied nonlinear optimization technique to obtain parameters. As the number of experimental points are not small and the data was not too noisy (as can be seen from the errors), we do not have the problem of over fitting here.

5. Results and discussion

Table 5 presents the values of the 20 UNIFAC interaction parameters determined between all possible functional group that could be part of the new adsorbent for radium adsorption. We can observed the strong interaction between radium and different groups such as water and sodium oxide since these parameters represent the energy of the interaction between the functional groups.

As mentioned before, these parameters were determined by fitting adsorption systems of four different adsorbents: Kaolinite, clinoptinolite, montmorillonite, and glauconite. The isotherms (calculated and experimental) of these systems are presented in Fig. 5. In this figure, we compared the capacity of adsorption (q^{exp}) from the experimental results and the calculated adsorption capacity (q^{cal}) with the interaction parameter shown in Table 5. It can be seen that the experimental and the estimated adsorption capacity values of q are in good agreement. These results are also reflected in the error function value obtained (i.e. 1.86e−4) which it corresponds to the value of the objective function shown in Eq. (33).

On the other hand, Table 6 reports the values of UNIFAC interaction parameters between all possible functional group that could be part of the new adsorbents for barium adsorption. In this case, the energy interaction of barium is very high especially with the anion chloride and the potassium oxide.

Similarity, we compared the capacity of adsorption for barium from the experimental (q^{exp}) and estimated (q^{cal}) values and the results can be shown in the isotherms of Figs. 6 and 7. The results are for the 3 adsorbents used: Ca-exchange clinoptilolite tuff, Ca-exchange montmorillonite clay and βMnO2. There is an excellent agreement between of the experimental and the estimated values of q with error values are 5.21e−10 for the first problem and 5.44e−12 for adsorption onto β-MnO_2 problem. Appendix 5 presents the Confidence interval calculation for the interaction parameters.

6. Conclusion

This is a first paper in the series of two papers to find an optimal adsorbent following computer-aided molecular design formulation. In this paper, we developed group contribution methods for barium and radium adsorption. The UNIFAC interaction parameters for the groups are computed using the available experimental isotherms for various adsorbents for barium and radium and an NLP optimization technique. These parameters are used to estimate the adsorption capacity at different

Table 5
Values of interaction parameter in the adsorption of radium.

Description	Variable	CI lower bound	Parameter value	CI upper bound
Bulk phase				
Ra–Na+	ab_{12}	Not sensitive	**8968.1**[a]	Not sensitive
Ra–Cl^-	ab_{13}	73.5 – 3.0774e – 06	**73.5**	73.5 + 3.0774e – 06
Ra–H_2O	ab_{14}	Not sensitive	**94335.5**[a]	Not sensitive
Na^+–Ra	ab_{21}	2020.8 – 4.2511e – 05	**2020.8**	2020.8 + 4.2511e – 05
Cl–Ra^-	ab_{31}	1335.7 – 5.7699e – 06	**1335.7**	1335.7 + 5.7699e – 06
H_2O–Ra	ab_{41}	6627.4	**6627.5**	6627.6
ASS Phase				
Ra–SiO_2	aa_{12}	– 846.7 – 1.8356e – 12	– **846.7**	– 846.7 + 1.8356e – 12
Ra–Al_2O_3	aa_{13}	– 3298.1 – 5.9439e – 12	– **3298.1**	– 3298.1 + 5.9439e – 12
Ra–Na_2O	aa_{14}	Not sensitive	**14,014.5**[a]	Not sensitive
Ra–MgO	aa_{15}	1161.9 – 7.4082e – 08	**1161.9**	1161.9 + 7.4082e – 08
Ra–Fe_2O_3	aa_{16}	796.5 – 4.7693e – 08	**796.5**	796.5 + 4.7693e – 08
Ra–K_2O	aa_{17}	– 1078.1 – 7.6953e – 12	– **1078.1**	– 1078.1 + 7.6953e – 12
Ra–CaO	aa_{18}	– 7410.9 – 2.3802e – 11	– **7410.9**	– 7410.9 + 2.3802e – 11
SiO_2–Ra	aa_{21}	– 71.2 – 7.4115e – 09	– **71.2**	– 71.2 + 7.4115e – 09
Al_2O_3–Ra	aa_{31}	6030.39	**6045.7**	6061.01
Na_2O–Ra	aa_{41}	4527.6	**4527.7**	4527.8
MgO–Ra	aa_{51}	– 620 – 2.4368e – 09	– **620**	– 620 + 2.4368e – 09
Fe_2O_3–Ra	aa_{61}	1988.8 – 3.1639e – 05	**1988.8**	1988.8 + 3.1639e – 05
K_2O–Ra	aa_{71}	6438.8	**6487.6**	6536.4
CaO–Ra	aa_{81}	474.7 – 1.0245e – 06	**474.7**	474.7 + 1.0245e – 06

Note: The values of interaction parameters are presented within their confidence interval CI. The value of the parameter is shown in bold. In some cases there was is no confidence interval, meaning that the results are very good and have tight bounds.

[a] The CI is not estimated since the objective function was insensitive to those parameters.

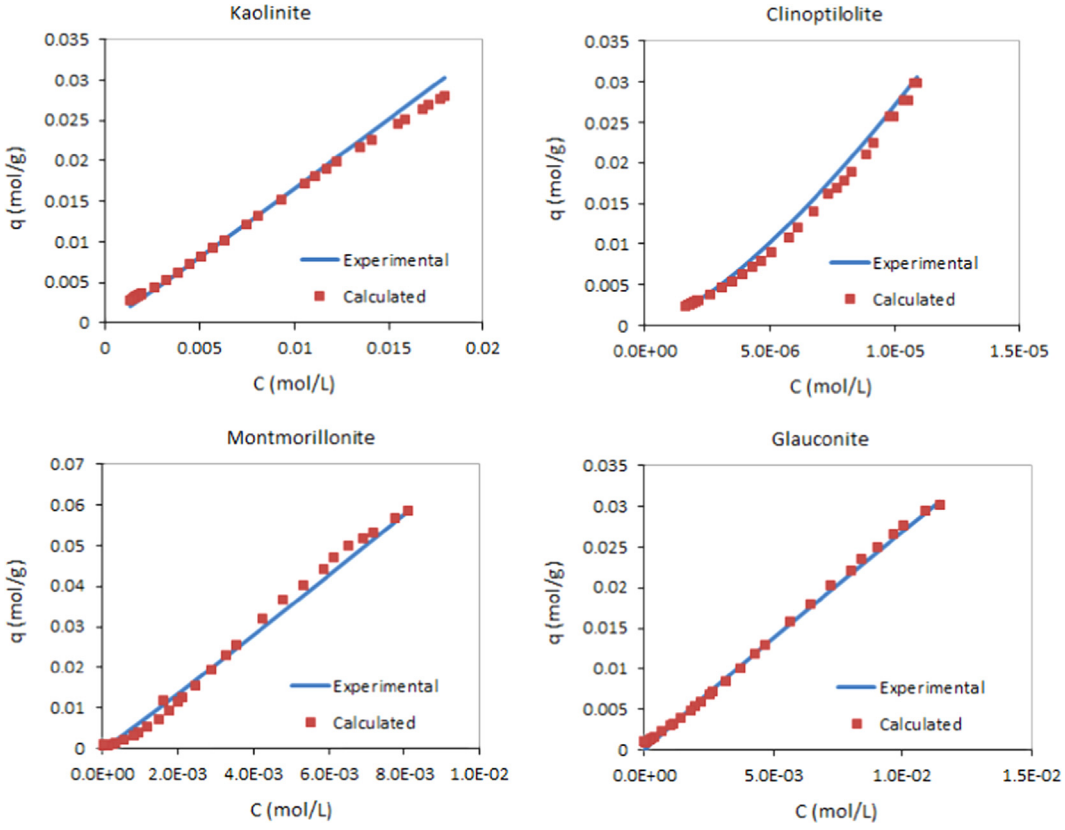

Fig. 5. Isotherm for adsorption of radium using Kaolinite, Clinoptinolite, Montmorrillonite and Glauconite. Comparison of the experimental adsorption capacity found in the literature and the calculated adsorption capacity.

concentrations and these parameter values are found to be in very good agreement with experimental results. In part 2 of the paper, we discuss the detail of the CAMD formulation and the optimization algorithms to find optimal adsorbents for the removal of barium and radium from produced waters from fracking.

Table 6
Values of interaction parameter in the adsorption of barium onto Ca-Cln and Ca-Mnt and onto β-MnO_2.

Bulk phase				
Description	Variable	CI lower bound	Parameter value	CI upper bound
Ba–Ca_2^+	ab12	−4109.7−7.7208e−10	**−4109.7**	−4109.7+7.7208e−10
Ba–Cl^-	ab13	Not sensitive	**47,935.9**[a]	Not sensitive
Ba–Na^+	ab15	4210	**4211.2**	4213
Ca_2^+–Ba	ab21	1033.9−1.7907e−02	**1033.9**	1033.9+1.7907e−02
Cl^-–Ba	ab31	−1536.6−8.8259e−07	**−1536.6**	−1536.6+8.8259e−07
Na^+–Ba	ab21	−42,726−7.8335e−10	**−42,726**	−42,726+7.8335e−10
ASS Phase				
Ba–SiO_2	aa12	1274.5	**1275.3**	1276
Ba–Al_2O_3	aa13	948.1	**949.2**	950.3
Ba–AlO_2^-	aa14	Not sensitive	**10,867.8**[a]	Not sensitive
Ba–FeO	aa15	−55,794−2.3249e−07	**−55,794**	−55,794+2.3249e−07
Ba–MgO	aa16	Not sensitive	**8872.1**[a]	Not sensitive
Ba–CaO	aa17	Not sensitive	**29,906.7**[a]	Not sensitive
Ba–Na_2O	aa18	−1870.32−1.6181e−08	**−1870.32**	−1870.32+1.6181e−08
Ba–K_2O	aa19	Not sensitive	**33,090.4**[a]	Not sensitive
Ba–Ca_2^+	aa110	−124,244−1.6013e−07	**−124,244**	−124,244+1.6013e−07
Ba–K^+	aa111	1402.6	**1418.7**	1434.7
Ba–βMnO_2	aa112	5710	**5712.9**	5716
SiO_2–Ba	aa21	Not sensitive	**6029.7**[a]	Not sensitive
Al_2O_3–Ba	aa31	Not sensitive	**2856.3**[a]	Not sensitive
AlO_2^-–Ba	aa41	Not sensitive	**6338.5**[a]	Not sensitive
FeO–Ba	aa51	−44,287.3−1.7231e−02	**−44,287.3**	−44,287.3+1.7231e−02
MgO–Ba	aa61	Not sensitive	**5044.6**[a]	Not sensitive
Ca0–Ba	aa71	Not sensitive	**−4072.6**[a]	Not sensitive
Na_2O–Ba	aa81	Not sensitive	**5685.7**[a]	Not sensitive
K_2O–Ba	aa91	Not sensitive	**−4564.8**[a]	Not sensitive
Ca_2^+–Ba	aa101	Not sensitive	**15,642.2**[a]	Not sensitive
K^+–Ba	a111	−44,279.4−6.6491e−04	**−44,279.4**	−44,279.4+6.6491e−04
β-MnO_2–Ba	aa121	−42,954.3−2.3863e−08	**−42,954.3**	−42,954.3+2.3863e−08

Note: The values of interaction parameters are presented within their confidence interval CI. The value of the parameter is shown in bold. In some cases there was is no confidence interval, meaning that the results are very good and have tight bounds.

[a] The CI is not estimated since the objective function was insensitive to those parameters.

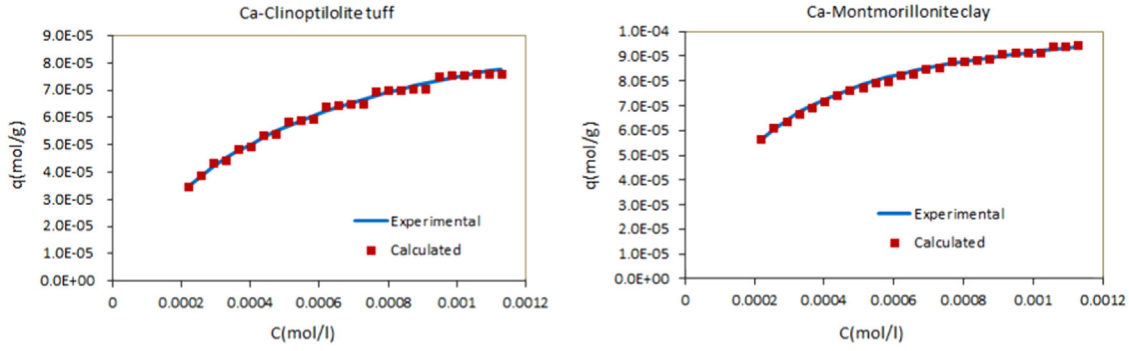

Fig. 6. Isotherm for adsorption of barium onto Ca-Cln and Ca-Mnt. Comparison of the experimental adsorption capacity found in the literature and the calculated adsorption capacity for barium adsorption.

Nomenclature

A_g	Van der Waals surface area (cm^2/mol)
a_{nm}	interaction parameters
b	Langmuir constant
C	equilibrium concentration in solution (mol/L)
C_I	initial concentration of radium in solution (mol/L)
Eq	total number of equation used to solve the problem
G^E	Gibbs excess free energy (J)
g^{ad}	free energy of immersion of the adsorbed solution (J/kg)
h_1, h_2	height of sphere segments (Å)
K	Langmuir constant
k_f	Freundlich constant
l	bond distances (Å)
m_0	mass of adsorbent (g)
M_0	molecular weight of Adsorbent (g/mol)
MW	molecular weight (g/mol)
ma	auxiliary parameter
N_{gt}	total functional groups
N_A	Avogadro number
n_f	Freundlich constant
J	jacobian
n	molar quantity (moles)
q	amount adsorbed for unit mass of adsorbent (mol/g)
q_i	parameter for Van der Waal surface calculation
Q_g	Van der Waals group surfaces of group K (m^2)

r_i parameter for Van der Waal volume calculation
r_w Van der Waals radius (Å)
r_1, r_2 : Var der Waals radii for both atoms (Å)
R_g Van der Waals group volumes of group K (m^3)
R ideal gas constant (8.314 J/mol K)
T temperature of adsorption (K)
vp pore volume of the adsorbent (cm^3/g)
v_{oi} molar volume of the respective fluid (cm^3/mol)
V_g Van der Waals volume (cm^3/mol)
V volume (L)
x molar fraction

Greek letters

γ activity coefficient
$\gamma^*_{GE,i}$ activity coefficient of a binary adsorbate-solid solution
φ^* chemical potential of the wetted solid adsorption of the pure component i (J/g)
φ^*_{oi} chemical potential of the wetted solid adsorption of the pure component i (J/g)
φ_i volume fraction for UNIFAC calculation
θ_i surface area fraction for UNIFAC calculation
Γ^s_{mi} surface phase capacity of component i (mol/g)
ρ density (g/ml)

Subscripts

i component i
0 adsorbent
1 adsorbate (radium or barium)
2, 3, 4 component 2, 3 or 4
$0i$ pure component i or pure adsorbed component i
g group index
j number of components
T total
Sln solution
H_2O water

Superscripts

$E*$ excess adsorbate-solid solution
Es excess of the surface phase
1 initial feed
b bulk phase
$*$ adsorbate solid solution
s surface phase
ad adsorption
C combinatorial
R residual in ASS
Cb combinatorial in bulk phase
Rb residual in the bulk phase
$C*$ combinatorial in ASS phase
$R*$ residual in the ASS phase
cal calculated
exp experimental

Acknowledgments

This work is financially supported by National Science Foundation under the Grant CBET-1434964. In addition, the authors want to thanks Dr. Berhane H. Gebreslassie and Dr. Rajib Mukherjee for their valuable suggestions and comments.

Appendix A1. Calculation of van der Waals volume and surface

The constants representing the group sizes and surfaces areas R_g and Q_g are obtained from atomic and molecular structural data, the van der Waals group volume V_g, and surface areas A_g, as it is shown in Eqs. (A1) and (A2) (Fredenslund et al., 1977).

$$R_g = V_g/15.17 \quad \text{(A1)}$$

$$Q_g = A_g/2.5e9 \quad \text{(A2)}$$

Where V_g and A_g are calculated from experimental data, namely, the so-called van der Waals radius (r_w) of each atom in the molecule representation

Radium (Ra). In the case of radium, a single spherical atom, the van der Waals volume is given by:

$$V_g = \frac{4}{3}\pi r_w^3 * N_A \quad \text{(A3)}$$

Where $r_w = 2.3$ Å equivalent to 2.3e−8 cm, and N_A is the Avogadro number equals 6.023e23moles/molecule, then $V_g = 30.696$ cm^3/mole. For the surface area value, Eq. (A4) is used:

$$A_g = \pi r_w^2 * N_A \quad \text{(A4)}$$

Then, $A_g = 1e9$ cm^2/moles.

Finally, replacing the values of V_g and A_g into Eq. A1 and Eq. (A2), respectively, we obtain $R_g = 2.023$ and $Q_g = 0.4$

Table A1 presents the van der Waals volume and surface values of radium and other components in the adsorption of radium.

Appendix A2. Functional groups of the adsorbents

For these two molecules, the geometrical method presented by Bondi (1968) is used to define the van der Waals volume and surface area. Apart from the van der Waals radii for both atoms (r_1, r_2), additional information related to the structure of the molecule is required, namely, the bond distances (1), an auxiliary parameter (ma), and the height of sphere segments (h_1, h_2). Eq.

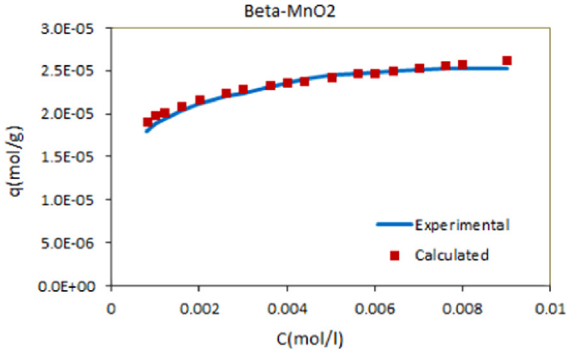

Fig. 7. Isotherm for adsorption of barium onto β-MnO_2. Comparison of the experimental adsorption capacity found in the literature and the calculated adsorption capacity for barium adsorption.

Table A1
Van der Waals volume and surface values.

Groups (g)	Amount of Groups	R_g	Q_g
Ra	1	2.023	0.4
Na^{+a}	1	3.0	3.0
Cl^{-a}	1	0.9861	0.9917
H_2O^a	1	0.92	1.40

[a] Values of R_g and Q_g can be found at Kikic and Fermeglia, (1991).

(A5) shows the van der Waals volume of diatomic molecule.

$$V_g = N_A\left(V_1^1 + V_2 - \Delta V_{2-1}\right) * 10^{-24} \ \text{cm}^3/\text{mole} \tag{A5}$$

where V_1^1, V_2 and ΔV_{2-1} are computed by Eqs. (A6)–(A8) and r is given in Angstrom units, then:

$$V_1^1 = \pi h_1^2\left(r_1 - \frac{h_1}{3}\right) \tag{A6}$$

$$V_2 = \frac{4}{3}\pi r_2^3 \tag{A7}$$

$$\Delta V_{2-1} = \pi h_2^2\left(r_2 - \frac{h_2}{3}\right) \tag{A8}$$

To compute the height of sphere segments, Eqs. (A9) and (A10) are used:

$$h_1 = r_1 + 1 - \text{ma} \tag{A9}$$

$$h_2 = r_2 - \text{ma} \tag{A10}$$

Finally, Eq. (A11) is used to calculate the auxiliary parameter ma:

$$\text{ma} = \frac{r_2^2 - r_1^2 + l^2}{21} \tag{A11}$$

On the other hand, the van der Waals surface area is computed using Eq. (A12):

$$A_g = 2\pi N_A(r_1 h_1 + 2r_2^2 - r_2 h_2) \tag{A12}$$

Once again, after V_g and A_g are calculated from the previous equations, these values are replaced into Eqs. (A1) and (A2), respectively. Table A2 summaries the result of these values for the groups of adsorbent used here.

Table A2
Information of functional groups of absorbents for calculation of R_g and Q_g.

Groups (g)	l (Å)	r_2 (Å)	r_1 (Å)	V_g (cm^3/mol)	A_g (cm^2/mol)	R_g	Q_g
SiO_2	1.61	2.1	1.52	21.067	3.167e9	1.388	1.268
Al_2O_3	1.935	1.84	1.52	16.829	2.759e9	1.109	1.104
MgO	2.11	1.73	1.52	15.368	2.602e9	1.013	1.041
Fe_2O_3	2.098	1.94	1.52	18.528	2.918e9	1.221	1.167
K_2O	2.86	2.75	1.52	41.198	4.609e9	2.716	1.844
Na_2O	2.41	2.27	1.52	25.600	3.517e9	1.688	1.407
β-MnO_2	1.922	1.26	1.52	10.731	2.036e9	0.707	0.815
(AlO_2)	1.641	1.84	1.52	16.673	2.753e9	1.099	1.101
CaO	2.4	2.31	1.52	26.576	3.594e9	1.752	1.438
FeO	2.17	1.94	1.52	18.580	2.920e9	1.225	1.168

Appendix A3. Structure and properties of the adsorbents for radium and barium removal

Table A3 presents the minerals used by Ames et al. (1983a, 1983b) with their chemical composition and molecular weight in the adsorption of radium. From this table, we can see the number of functional groups that are contained in each adsorbent. The first four adsorbents belong to the clay mineral group also known as hydrous aluminum phyllosilicates. The word "clays" was assigned early to fine grained material in geological formations or soils with size less than 2 μm (Velve and Meunier, 2008). The clinoptilolite is one of the most abundant natural zeolite. It has been used for radioactive waste disposal and ammonia recovery from sewage effluents (Yang, 2003). The last adsorbent is silica gel which is most-used as a desiccant or adsorbent for moisture (Yang, 2003). For the chemical analysis of these minerals see Ames et al. (1983a, 1983b). The calculation of the molecular weight for all clays was based on the chemical structure general formula (Deer et al., 1992).

On the other hand, Table A4, presents the chemical structure and molecular weight of the adsorbents used for adsorption of barium. Clinoptinolite tuff (Ca-Cln) is constituted by clinoptinolite–heulandite and mordenite with minor plagioclase, feldspar, cristobalite, quartz, and glass. The montmorillonite clay (Ca-Mnt), on the other hand, contains ~85% of montmorillonite associated with plagioclase, feldspar, glass, opal, and calcite. Beta-manganese oxide was also studied for the adsorption of barium. For more information about the adsorbent's composition please refer to Chavez et al. (2010) and Arafa et al. (1974) The molecular weight is calculated based on the chemical composition presented by the authors.

Appendix A4. Calculation steps to compute the adsorption capacity for Kaolinite

Table A5 summarizes the important calculations followed to compute the adsorption capacity (q^{cal}) for Kaolinite. The table presents the expression used, its value and the equation used to demonstrate one point of Fig. 5 (i.e. when concentration (C) in the equilibrium is equal to 0.018 mol/L). We used the interaction parameters for Kaolinite shown in Table A6, which are also presented in Table 5 for all the interaction parameters involved in the adsorption of radium.

Appendix A5. Confidence interval calculation of the interaction parameters

Reliability of the parameters is obtained by finding the confidence interval (Rasmuson et al., 2014). The approximate

Table A3
List of secondary mineral used in adsorption of radium and their molecular weight and pore volume values.

Absorbent	Structure	Pore volume, vp (cm^3/g)	M_0 (g/mol)	Type of mineral	Reference
Kaolinite	$(Al_2O_3)(SiO_2)_2(H_20)$	0.278	222.127	Clay-mica group/phyllosilicate	Diamond, (1970) and Benco et al. (2001)
Montmorillonite	$(Na_2O)\ (MgO)_2\ (Fe_3O_2)\ (Al_2O_3)_2\ (SiO_2)_4\ {}_2H_2O$	0.172	786.374	Clay-mica group/phyllosilicate	Diamond (1970)
Nontronite	$(Na_2O)(Fe_2O_3)(Al_2O_3)_2(SiO_2)_4 \cdot {}_2H_2O$	0.255	665.920	Clay-mica group/phyllosilicate	Diamond (1970)
Glauconite	$(K_2O)(MgO)_2(Fe_2O_3)(Al_2O_3)_2(SiO_2)_4$	0.164	778.736	Iron potassium phyllosilicate	Hassan and El Shall (2004)
Clinoptilolite	$(CaO)(Na_2O)(K_2O)(Al_2O_3)_3(SiO_2)_{30.24}H2O$	0.186	2320.62	Natural Zeolite	Yang (2003)
Silica gel	(SiO_2)	0.43	60.083	Silica	Yang (2003) and Ruthven (1984)

Table A4
Information about the adsorbents used in adsorption of barium.

Absorbent	Structure	M_0 (g/gmol)	Type of mineral	Reference
Clinoptilolite tuff (Ca-Cln)	$(K^+)(Ca^{+2})(K_2O)(Na_2O)(CaO)\ (AlO_2)_2^-\ (Al_2O_3)_{3.1}(SiO_2)_{37.9}(H_2O)_{24}$	187.207	Natural zeolite	Chavez et al. (2010)
Montmorillonite (Ca-Mnt)	$(Na_2O)\ (MgO)_2\ (FeO)\ (Al_2O_3)_2\ (SiO_2)_4\ {}_2H_2O$	399.104	Clay	Chavez et al. (2010)
Beta-Manganese oxide	β-Mn_2O	86.937	Oxides	Arafa et al. (1974)

Table A5
Calculation steps to compute the adsorption capacity for Kaolinite.

Description	Expression	Value	Source
Temperature (K)	T	298.15	Ames et al. (1983a, 1983b)
Volume of solution (L)	V_{sln}	1	Assume
Ideal constant (J/mol K)	R	8.314	Literature
Pore volume (cm^3/g)	vp	0.278	Table A3
Surface-phase capacity of Ra in Kaolinite (mol/g)	Γ^s_{mi}	0.0068	Eq. (4)
Molecular weight of solid (g/mol)	M_0	222.127	Table A3
Amount of solid (g)	m_0	50	Ames et al. (1983a, 1983b)
Activity coefficient for the pure component	γ^*_{01}	1.66213	Eq. (11)
Initial concentration of radium (mol/L)	C_I	2.95	Ames et al. (1983a, 1983b)
Initial moles of radium (mol)	n^1_1	2.95	Eq. (19)
Moles of adsorbate solid solution phase for radium (mol) (using the q from Ames et al. (1983a, 1983b))	n^*_1	1.516	Eq. (17)
Moles of adsorbent in the adsorbate solid solution (mol)	n^*_0	0.225096	Eq. (16)
Moles of bulk phase (mol)	n^b_1	1.433	Eq. (18)
	n^b_2	0.01	$C_{NaCl}*V_{sln}$
	n^b_3	48.76	$(V_{H_2O}*\rho_{H_2O})/\ MW_{H_2O}$
Mole fraction of adsorbent solid solution	x^*_0	0.1292	Eq. (21)
	x^*_1	0.8708	
Mole fraction of bulk phase	x^b_1	0.0285	Eq. (20)
	x^b_2	0.0002	
	x^b_3	0.9713	
Mole fraction of surface phase	x^s_1	1	Eq. (10)
Activity coefficient from bulk phase	$\ln \gamma^b_1$	10.1494	Eq. (22)
	$\ln \gamma^b_2$	−8.8833	
	$\ln \gamma^b_3$	0.0213	
Activity coefficient from adsorbate solid solution	$\ln \gamma^*_1$	0.1768	Eq. (12)
	$\ln \gamma^*_0$	−8.5292	
Gibbs excess free energy (J)	G^{E*}	−3765.57	Eq. (35)
	G^{Es}	0	Eq. (36)
	G^{E*}_{0i}	1757.235	Eq. (37)
Difference of the chemical potential (J/g)	$\varphi^* - \varphi^*_{oi}$	−110.456	Eq. (39)
Total moles in the adsorbate solid solution (using the interaction parameters)	n^*_T	1.6024	Eq. (38)
Adsorption capacity calculated	q^{cal}	0.0279	Eq. (34)
Adsorption capacity experimental	q^{exp}	0.0303	Ames et al. (1983a, 1983b)

confidence interval is obtained by linearization of the nonlinear function with a first order Taylor series expansion around the estimated parameter using Eq. (A13):

$$f(x_n,\theta) = f\left(x_n,\hat{\theta}\right) + \frac{\partial f\left(x_n,\hat{\theta}\right)}{\partial \theta_p}_{\theta-\hat{\theta}} (\theta-\hat{\theta}) \tag{A13}$$

where $\hat{\theta}$ is the estimated parameter.

The first order derivative of the nonlinear function is the Jacobian. It can be represented as shown in Eq. (A14)

$$J_{n,p} = \frac{\partial f\left(x_n,\hat{\theta}\right)}{\partial \theta_p}_{\theta-\hat{\theta}} \tag{A14}$$

where n is the experimental point where the derivative is taken and p is the parameter.

Since it is difficult to find the Jacobian theoretically, a numerical estimation can be done. The approximation of the Jacobian is done as follows: the parameters $\hat{\theta}$ where sum of square error (SSE) has been identified from the optimization problem where SSE has been minimized. At the optimal point of the parameters, one parameter is changed at a time by 1%, (denoted by $\hat{\theta}_{p,1\%}$). All other parameters remain at the minima. The function is calculated at this point. Then, this parameter is changed back to original and the next parameter is changed by 1% and the function is calculated.

Table A6
Unifac interaction parameters for Kaolinite.

Parameter	Value
Ra–Na^+	8968.14
Ra–Cl^-	73.45
Ra–H_2O	94335.54
Na^+–Ra	2020.83
Cl–Ra	1335.69
H_2O–Ra	6627.52
Ra–SiO_2	−846.70
Ra–Al_2O_3	−3298.09
SiO_2–Ra	−71.19
Al_2O_3–Ra	6045.72

The approximate numerical estimation of the Jacobian is given by Eq. (A15):

$$J_{n,p} = \frac{f\left(x_n, \hat{\theta}\right) - f\left(x_n, \hat{\theta}_{p,1\%}\right)}{\Delta\theta_p} \tag{A15}$$

The $1-\alpha$ confidence interval for $\hat{\theta}_p$ is determined by Eq. (A16)

$$\hat{\theta}_p \pm se\left(\hat{\theta}_p\right) t(n-p, \alpha/2) \tag{A16}$$

where $t(n-p, \alpha/2)$ is the Student's t distribution with $n-p$ degrees of freedom and $\mathrm{se}\left(\hat{\theta}_p\right)$ is the standard error for parameter calculated using Eq. (A17)

$$\mathrm{se}\left(\hat{\theta}_p\right) = s\sqrt{\left(\left(J^{\mathrm{T}}J\right)^{-1}\right)_{pp}} \tag{A17}$$

where s is the standard deviation obtained from the objective function SSE

$$s = \sqrt{\frac{\mathrm{SSE}}{n-p}} \tag{A18}$$

For some cases the confidence interval is very tight due to very small hessian. For cases where the Hessian is very large, the confidence interval is very large and the objective function is insensitive to the parameter changes.

References

Ames, L., McGarrah, J., Walker, B., 1983a. Sorption of trace constituents from aqueous solutions onto secundary minerals. Radium ll. Clays Clay Miner. 31, 335–342.

Ames, L., Mc.Garrah, J., Walker, B., 1983b. Sorption of trace constitutes from aqueous solutions onto secondary minerals. l uranium. Clays Clay Miner. 31, 321–334.

Arafa, M., Yousef, A., Malati, M., 1974. Adsorption of barium ions by Beta_Manganese dioxide and its activation in oleate flotation. Int. J. Miner. Process. 1, 267–275.

Benco, L., Tunega, D., Hafner, J., Li, H., 2001. Upper limit of the O–H–O hydrogen bond. Ab initio study of the Kaolinite structure. J. Phys. Chem. 105, 10812–10817.

Benavides, P., Diwekar, U., Gebreslassie, B., 2015. Optimal design of adsorbents for NORM removal from produced water in natural gas fracking. Part 2: CAMD for adsorption of radium and barium Submitted for publication. Chem. Eng. Sci..

Berti, C., Ulbig, P., Burdorf, J., Seippel, J., Schulz, S., 1999. Correlation and prediction of liquidi-phase adsorption on zeolites using group contribution methods based on the adsorbate-solid solution theory. Langmuir 15, 6035–6042.

Berti, C., Ulbig, P., Schulz, S., 2000. Correlation and prediction of adsorption from liquid mixtures on solids by use of GE-Models. Adsorption 6, 79–91.

Bondi, A., 1968. Physical Properties of Molecular Crystals, Liquids, and Glass. John Wiley & Sons, New York.

Chavez, M., Pablo, L., Garcia, T., 2010. Adsorption of Ba^{+2} by Ca-exchange clinoptilolite tuff and montmorillonite clay. J. Hazard. Mater. 175, 216–223.

Deer, W., Howie, R., Zussman, J., 1992. An Introduction to the Rock-forming Minerals, 2nd ed. Prentice Hall, England.

Diamond, S., 1970. Pore size distributions in clays. Clays Clay Miner. 18, 7–23.

Fredenslund, A., Gmehling, J., Rasmussen, P., 1977. Vapor–liquid Equlibria Using UNIFAC A Group Contribution Method. Elsevier Scientific Publishing Company, Amsterdam.

Hassan, M., El Shall, H., 2004. Glauconitic clay of El Gidida Egypt: evaluation and surface modification. Appl. Clay Sci. 27, 219–222.

Joback, K., Reid, R., 1987. Estimation of pure-component properties from group-contributions. Chem. Eng. Commun. 57, 233–243.

Kikic, I., Fermeglia, M., 1991. UNIFAC prediction of vapor–liquid equilibria in mixed solvent-salt systems. Chem. Eng. Sci. 46, 2775–2780.

Lydersen., 1955. Estimation of Critical Properties of Organic Compounds. College Enineering University Wisconsin. Engineering Esperimental Station Report 3. Madison.

Lustgarten., 2009. Frack Fluid Spill in Dirmock Contaminantes Stream, Killinf Fish. Propublica. ⟨www.propublica.org/article/frack-fluid-spill-in-dimock-contaminantes-stream-killing-fish-921⟩.

Marcellus Shale., 2011. Understanding naturally occurring radioactive material in the Marcellus Shale. Issue 4 ⟨http://www.museumoftheearth.org/files/marcellus/Marcellus_issue4.pdf⟩.

Marrero, J., Gani, R., 2001. Group-contribution based estimation of pure component properties. Fluid Phase Equilibria 183, 183–208.

Purdey, M., 2004. Chronic barium intoxication disrupts sulphated proteoglycan synthesis: a hypotesis for the origins of multiple sclerosis. Med. Hypotheses 62, 746–754.

Rasmuson, A., Andersson, B., Olsson, L., Andersson, R., 2014. Mathematical Modeling in Chemical Engineering. Cambridge University Press, United Kingdom.

Replica Engineering INC., 2014. ⟨http://www.replicaeng.com/Replica-Engineering/Hydraulic-Fracturing/Marcellus-Shale-Formation.htm⟩.

Rowan, E., Engle, M., Kirby, C., Kraemer, T., 2011. Radium Content of Oil- and Gas-Field Produced Waters in the Northern Appalachian Basin (USA)-Summary and Discussion of Data. Scientific investigations Report. U.S. Geological Survey, Reston, Virginia.

Ruthven, D., 1984. Principles of Adsorption and Adsorption Processes. John Wiley & Son, Canada.

Silva, J., Matis, H., Kostedt, W., Watkins, V., 2012. Produce Water Preatrement for Water Recovery and Salt Production. General Electric Global Research Center, Niskayuna, New York.

Smith, T., 2012. Environmental considerations of shale gas development. Chem. Eng. Process. 108, 53–58.

Suzuki, M., 1990. Adsorption Engineering. Elsevier Science Publishing Company, INC, New York.

U.S. Department of Energy Website, 2014a. E. I. US Energy Information Administration. DOE-EIA. http://www.eia.gov/naturalgas/.

U.S. Department of Energy Website, 2014b. E. I. Annual Energy Outlook 2014, Early Release Overviwe. Retrieved from U.S. Department of Energy, Energy Information Administrative. ⟨http://www.eia.gov/forecasts/aeo/er/pdf/0383er(2014).pdf⟩.

U.S.EPA., 2014. Environmental Protection Agency, EPA. ⟨http://www.epa.gov/safewater/agua/estandares.html⟩.

Velve, B., Meunier, A., 2008. The Origin of Clay Minerals and Soils and Weathered Rocks. Springer-Verlag, Berlin Heidelberg, Paris.

Warner, N., Christie, C., Jackson, R.B., Vengosh, A., 2013. Impacts of shale gas wastewater disposal on water quality in western Pennsylvania. Environ. Sci. Technol. 47, 11849–11857.

Yang, P., 2003. Adsorbents: Fundamentals and Applications. John Wiley & Sons, Hoboken, New Jersey.

Zielinski, R., Otton, J., 1999. Naturally Ocurring Radioactive Materials (NORM) in produce water and oil-field equiment- an issue for the energy industry. USGS, science for a changing world. Geological Survey. Denver, CO.